Journal of Building Engineering 72 (2023) 106575

Contents lists available at ScienceDirect

Journal of Building Engineering

journal homepage: www.elsevier.com/locate/jobe

High temperature performance of geopolymers based on construction and demolition waste

Ioanna Giannopoulou [a, *], Ponsian M. Robert [a, b], Konstantinos-Miltiadis Sakkas [c], Michael F. Petrou [d], Demetris Nicolaides [a, b, **]

[a] Frederick Research Center, 7, Filokyprou Str. Pallouriotisa, Nicosia, 1036, Cyprus
[b] Frederick University, Department of Civil Engineering, 7, Y. Frederickou Str. Pallouriotisa, Nicosia, 1036, Cyprus
[c] RECS Engineering, Griva Digeni Av., Lakatamia, Nicosia, 2450, Cyprus
[d] University of Cyprus, Department of Civil & Environmental Engineering, 75 Kallipoleos Av., P.O. Box 20537, Nicosia, 1678, Cyprus

ARTICLE INFO

Keywords:
Construction and demolition waste
Geopolymer
Thermal stability
Fire resistance

ABSTRACT

This paper reports an experimental study on the thermal stability and mechanical performance of geopolymers developed entirely with construction and demolition waste precursors, either bricks or ceramic tiles, upon their firing at temperatures between 600 and 1050 °C. The waste brick- and waste tile-based geopolymers were prepared with solid to liquid ratios of 2.4 and 3.4, respectively, using combined aqueous solutions of potassium hydroxide (KOH) and sodium silicate (Na_2SiO_3), as alkali activator. After curing for 7 days at 50 °C and hardening for 7 and 28 days at ambient temperature, the geopolymers were exposed to 600, 800 and 1050 °C for 2 h and their compressive strength, apparent density and mass loss were measured. Both materials showed good thermal stability up to 1050 °C, without observing any change in the shape of specimens or thermal deformation. The waste brick-based geopolymer developed a compressive strength of about 19 MPa after ageing for 7 days and kept it in the range of 15–21 MPa, after its exposure to 600–1050 °C. At 1050 °C, the material showed a decreased density by 8% and mass loss about 10%. The compressive strength of the waste ceramic tile-based geopolymer was about 33 MPa after 7 days of hardening and decreased to about 17 and 13 MPa, after exposure to 600 and 800 °C, respectively. At 1050 °C, its compressive strength was slightly increased compared to the initial one. At this temperature, the density of the material decreased by almost 9%, while it lost about 7% of its initial mass. Based on these results, both the developed geopolymers had the potential to find fire resistance applications in the sector of building materials.

1. Introduction

Geopolymers are innovative and pioneering materials produced through the alkali activation of solid aluminosilicate sources rich in reactive silica and alumina. As alkali activators, aqueous solutions of sodium or potassium hydroxide, combined with soluble silicates are used. The geopolymerization process comprises a sequence of complex chemical reactions that take place at relatively low temperatures (up to 100 °C), involving the formation of a partially or totally amorphous three-dimensional network, which consists of polymer chains of Si or Si/Al atoms linked through bridging atoms of oxygen (Si–O-*T*, where *T* denotes Si or Al) [1,2]. This specific polymeric structure classifies geopolymers as inorganic polymers, while it provides them with excellent physical, chemical, mechani-

* Corresponding author.
** Corresponding author. Frederick Research Center, 7, Filokyprou Str. Pallouriotisa, Nicosia, 1036, Cyprus.
E-mail addresses: ioangian@outlook.com (I. Giannopoulou), d.nicolaides@frederick.ac.cy (D. Nicolaides).

https://doi.org/10.1016/j.jobe.2023.106575
Received 24 February 2023; Received in revised form 12 April 2023; Accepted 14 April 2023
Available online 15 April 2023

cal and thermal properties, such as low porosity, negligible water permeability, adsorption capacity, resistance to chemical corrosion and high temperature, high early mechanical strength and low thermal conductivity [3–7]. Due to these properties, geopolymers are suitable to be used as ceramics, binders for pre-casting, coatings and other building and construction materials [3,6,8–13] or as matrices for the encapsulation of hazardous and toxic substances [14–16].

There is a variety of solid aluminosilicate sources that can be used for geopolymers manufacturing, including natural clays and minerals [17,18], and waste materials and by-products generated in huge quantities every year worldwide, such as fly ashes and metallurgical slags [3,8–12], waste glass and construction and demolition waste [7,19–24]. Among them, metakaolin, fly ash from thermal power plants, slags from the ferrous industry and the red mud from the alumina production are the most investigated. On the other hand, the geopolymerization of construction and demolition waste (CDW) still remains challenging, although it is categorized as one of the most voluminous solid waste worldwide. In the European Union (EU) countries, more than 800 million tons of CDW are generated every year, which constitutes approximately one-third of the total industrial and urban waste generated annually in the EU [25]. It has to be underlined that the European Commission has characterised CDW as a priority waste stream for reuse and highlighted the important environmental benefits derived from their valorization, such as saving of natural resources, reduction of GHG emissions and minimization of waste landfilling. CDW comprises a variety of materials, including concrete, bricks, tiles, gypsum, wood, glass, metals and plastic. The high SiO_2 and Al_2O_3 contents in certain materials among them, such as bricks, ceramic tiles and concrete, make their utilization in the production of geopolymers interesting.

Although there was intensive research on the development of geopolymers to be used as building materials over the past two decades, the relevant studies focused mainly on materials with improved mechanical properties at ambient conditions. A rather limited number of the published research papers are referred to the thermal performance and mechanical properties of geopolymers, after high-temperature exposure. The most important factors affecting the thermal stability and mechanical performance of geopolymers after their exposure at elevated temperatures include the type of the geopolymeric precursor and the used aggregates, the molar ratio Si/Al, the alkali cation and the total alkali content in the geopolymeric system, as well as the heating rate [26–28]. Relevant studies reported particular thermal stability of geopolymers based on metakaolin and sodium or potassium silicate/hydroxide solutions, when they were properly cured to retain the amorphous structure up to their melting temperature [29,30] or when proper molar ratios Si/Al were selected, to promote the formation of specific crystalline phases with high melting points [31]. As it is noted, the amount of formed crystalline phases at high temperatures decreased with the increasing Si/Al ratio, regardless of the alkali cation existing in the system (Na, K or Na–K) [32], while uncompleted crystallization of the amorphous geopolymeric phase reduced the mechanical strength of the obtained materials [11]. Regarding the type of alkali cation, it was observed that the K-based geopolymers experienced minimum thermal deformation at elevated temperatures, followed by the Na/K- and the Na-based ones, respectively [32]. In addition, the high-temperature properties of geopolymers, such as the temperature of crystallization and sintering, the residual compressive strength and the thermal resistance, were strongly affected by the total alkali content in the geopolymeric system [26]. The residual compressive strength of geopolymers based on metakaolin or fly ash or on their mixtures decreased with the increase of the exposure temperature, while the relevant specimens presented few visible cracks but no spalling phenomena [8,27–34]. Similarly, the compressive strength of geopolymers prepared through the alkali activation of granulated Ca-rich blast furnace slag (BFS) decreased by about 40% of its initial value, after exposure to 1200 °C for 1 h, while the flexural strength of the same materials exceeded its initial value by 17% and 80%, after exposure at 1000 and 1200 °C, respectively [35]. Furthermore, the reverse-side temperature of the BFS-based geopolymers exposed to an 1100 °C flame equilibrated at less than 400 °C after 35 min [13]. Similarly, the geopolymers based on the activation of ferronickel slag with potassium hydroxide and soluble silicate solutions presented excellent fire resistance, when tested according to the RWS (Rijkswaterstaat) temperature-time curve and proved able to withstand successfully a fire under such severe conditions [36,37]. Combinations of fly ash and slag in different ratios were also used to prepare geopolymers that were exposed at high temperatures, up to 800 °C [38]. The residual strength of the obtained materials decreased exponentially, as their initial strength was increased and this behavior was attributed to the reduced ductility of the materials that was observed with the increase of their initial strength.

Due to their chemistry and microstructure, geopolymers have inherent fire resistance that enhances their use in high temperature applications [26]. The unique inorganic network that comprises the backbone of geopolymers structure renders them non-combustible, while they are also non-smoking and non-toxic materials. Geopolymers contain large amounts of physically and chemically bound water that migrates and evaporates at high temperatures, providing them with endothermic properties. Given that their mechanical strength can reach and exceed 100 MPa [9], geopolymers can serve as fireproofing building materials with immense potential for applications in extreme conditions, where enhanced mechanical and fire resistance performance is required.

This paper investigates the potential of developing fire-resistant geopolymers based entirely on waste bricks (WB) and waste ceramic tiles (WCT). More precisely, it studies the thermal stability and mechanical performance of optimized WB- and WCT-based geopolymers after their exposure to temperatures up to 1050 °C, in terms of compressive strength, apparent density and mass loss. The specimens of geopolymers exposed to the studied temperatures were also visually investigated and the observed microcracks or other surface defects or spalling phenomena and damages are reported, as well. The present research combines the benefits of developing sustainable materials based on the utilization of secondary raw materials, such as the CDW, with decreased demand for natural resources and demonstrates a new low-cost processing route to produce advanced materials for the effective passive fire protection of buildings. According to the results, the recycling of the studied CDW streams in the production of fire-resistant geopolymers for buildings and construction applications, is very promising.

2. Materials and methods

2.1. Raw materials

Two types of CDW, waste bricks (WB) and waste ceramic tiles (WCT) were selected in this study to be used as precursors for the development of the fire-resistant geopolymers. Both of these waste materials were delivered from a recycling plant of CDW in Cyprus, named Resource Recovery Cyprus (RRC). After manual sorting, the broken waste bricks and waste ceramic tiles were crushed and ground to achieve homogeneous powders with reduced particle size. In Fig. 1, the geopolymer precursors used in the current study, as received from the recycling plant and after crushing and grinding are presented.

The particle size distribution (PSD) curves of WB and WCT are shown in Fig. 2. Each PSD diagram given in Fig. 2 has been derived from the average of 13 reproducible measurements performed with the relevant number of samples of the corresponding raw material. According to Fig. 2, WB is slightly finer than the WCT; in particular, the particle size of WB is lower than 250 μm, with a mean diameter d_{50} = 35.35 μm, while the particle size of WCT is lower than 300 μm, with a mean diameter d_{50} = 48.34 μm.

Table 1 presents the chemical analysis of WB and WCT performed by the X-Ray Fluorescence method (ED-XRF spectrometer SPECTRO XEPOS). The concentrations of the oxides given in Table 1 are the mean values that were taken from 13 reproduced analyses carried out for each raw material. Table 1 includes also the standard deviations (SDs) of these sets of values per oxide and

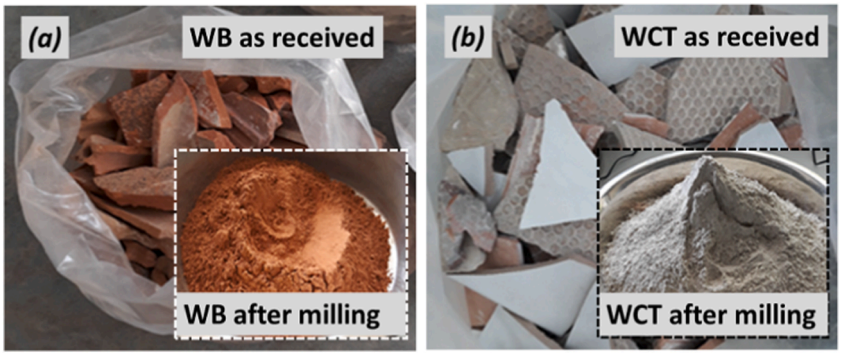

Fig. 1. (a) Waste Brick (WB) and (b) Waste Ceramic Tile (WCT) used in this study.

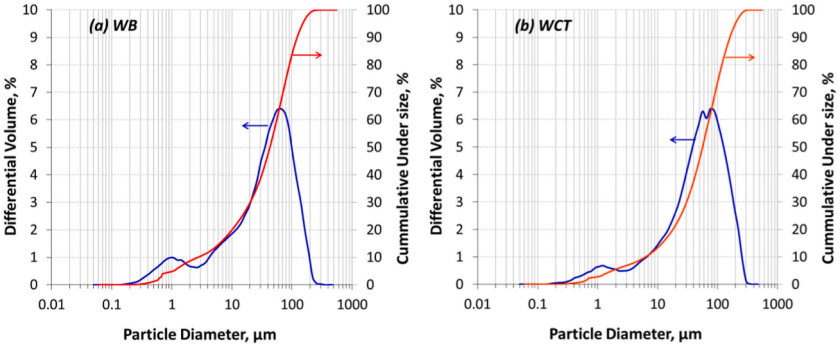

Fig. 2. Particle size distribution curves of (a) WB and (b) WCT.

Table 1
Chemical analysis of WB and WCT.

Oxide	WB		WCT	
	% wt.	SD	% wt.	SD
SiO_2	53.57	4.92	62.40	4.46
Al_2O_3	14.33	4.09	14.68	3.93
CaO	7.71	2.70	1.48	1.42
FeO	10.19	1.91	8.58	0.93
K_2O	3.74	1.16	3.76	1.96
MgO	4.07	1.97	3.68	2.52
Na_2O	0.66	0.54	0.98	1.74
TiO_2	1.46	0.94	–	–

raw material. According to Table 1, both of the geopolymer precursors (WB and WCT) are rich in silicon oxide, the content of which is lower in the WB (53.57 %wt.) than in the WCT (62.40 %wt.). Both of these raw materials have also high and quite similar contents of aluminum oxide (about 14 %wt.), as well as of iron oxide (10.19 and 8.58 %wt. for WB and WCT, respectively), potassium oxide (about 3.75 %wt.) and magnesium oxide (near 4 %wt.), as shown in Table 1. In addition, both the geopolymer precursors contain calcium oxide, which is much higher in WB (7.71 %wt.) than in WCT (1.48 %wt.), and traces of sodium and titanium oxides in WB (Table 1).

The mineralogical analysis of WB and WCT was performed by X-Ray Diffraction (XRD) method (D8 Bruker Diffractometer, CuKα radiation, $\lambda = 1.5418$ nm) in the range of 2theta between 2° and 70° with a scanning speed of 2°/min and the results are shown in Figs. 3 and 4, respectively.

According to Fig. 3, the main mineralogical phases found in WB are attributed to feldspars (anorthite-$CaAl_2Si_2O_8$ and albite-$NaAlSi_3O_8$) and quartz (SiO_2). In addition, hematite (Fe_2O_3) was identified as secondary phase, while diopside ($MgCaSi_2O_6$) and mullite ($3Al_2O_3{\cdot}2SiO_2$) as minor phases (Fig. 3). Quartz (SiO_2) was also identified as the major crystalline constituent of WCT (Fig. 4), with K-feldspars (orthoclase-$KAlSi_3O_8$), hematite (Fe_2O_3), mullite ($3Al_2O_3{\cdot}2SiO_2$) and spinel ($MgAl_2O_4$) to contribute as minor phases. As seen in Fig. 4, WCT contains also an amorphous phase indicated by the broad hump registered in 2theta between 20° and 30°. It is an aluminosilicate phase also found in other raw materials used in geopolymers, such as metakaoline, fly ash and slag [33–35], which indicates the suitability of WCT to be used as geopolymer precursor.

The density (bulk and apparent) and water absorption of WB and WCT were measured according to ASTM 128-88. Based on the results, the bulk and apparent densities of WB were 1.63 g/cm^3 and 2.81 g/cm^3 respectively, while its water absorption was 25.57%. The WCT had lower water absorption than WB (15.77%), while its bulk and apparent densities were relatively similar to those of WB and equal to 1.82 g/cm^3 and 2.56 g/cm^3, respectively.

The alkaline activator used in this study consisted of potassium hydroxide (KOH) solution and sodium silicate solution (MERCK, $Na_2O = 8\%$, $SiO_2 = 27\%$ and $d = 1.346$ g/mL). The KOH solution was prepared by dissolving KOH anhydrous pellets of analytical grade (MERCK, 99.5% purity) in distilled water and its concentration was selected to be 8 mol/L (M) in all the experiments, considering that at lower alkaline concentrations the content of OH^- ions is inadequate to facilitate the dissolution of silicate and aluminate phases and therefore promote geopolymerizations [33]. Since the materials focused in this study are intended to be used for the passive fire protection of buildings, KOH was selected over NaOH for the alkali-activating solution, given that the potassium-based geopolymers withstand at temperatures higher than 1200 °C and remain durable during and after a fire [37]. Leucite ($KAlSi_2O_6$),

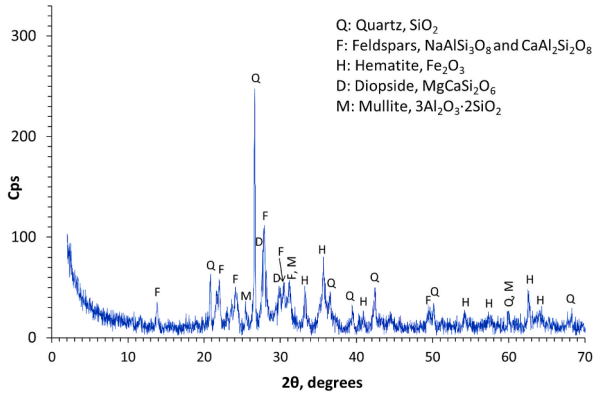

Fig. 3. XRD analysis of waste brick (WB).

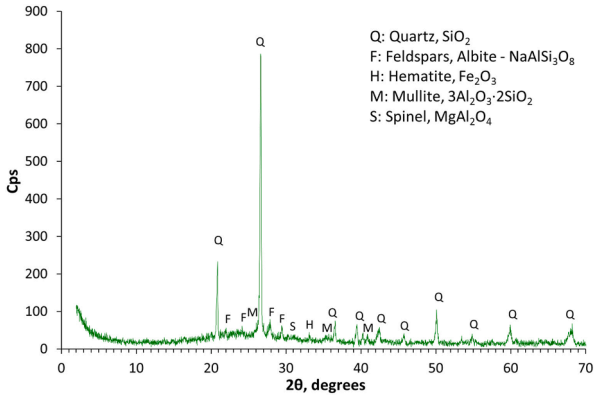

Fig. 4. XRD analysis of ceramic tile waste (WCT).

which is a potassium aluminosilicate phase formed in the K-based geopolymeric systems at about 1150 °C [26,32], has eutectic temperature higher than 1500 °C. On the opposite, nepheline ($NaAlSiO_4$), which is a sodium aluminosilicate phase formed in the Na-based geopolymeric systems at about 800–900 °C, is stable up to about 1000–1100 °C [30–32].

2.2. Experimental procedure

The geopolymers Brick Fire Resistant (BFR) and Ceramic Tiles Fire Resistant (CTFR) were prepared by mixing the solid precursor, either WB or WCT, respectively, with the alkaline activating solution in a mechanical mixer for 5 min to form a homogeneous paste. The obtained geopolymeric pastes were then cast in open steel cubic molds with two sets of dimensions, 50 × 50 × 50 mm and 100 × 100 × 100 mm. The formed specimens were left for curing at 50 °C for 7 days, under atmospheric pressure and non-controllable humidity conditions. When the curing process has been completed, the cubic specimens were demolded and left for hardening at ambient temperature and dry conditions for 7 and 28 days, before the measurement of the compressive strength, density and mass loss and the performance of FTIR analysis.

In order to elucidate the capability of the developed geopolymers BFR and CTFR to withstand high temperatures, they were subjected to firing at 600, 800 and 1050 °C for 2 h, using a laboratory electric furnace (Fig. 5). In each experiment, the specimens of geopolymers were placed in the furnace (Fig. 5) that started from room temperature to reach the desired temperature, operating with a heating rate of 4.4 °C/min. The specimens were left at the predefined temperature for 2 h and then, the furnace was turned off and the specimens were left in the furnace for cooling to room temperature, under open air conditions. After each experiment, the structural integrity of geopolymers was assessed by means of compressive strength, density and mass loss measurements, while the structural rearrangements that took place in their matrices were evaluated according to FTIR analysis. Cubic specimens with the dimensions of either 50 × 50 × 50 mm or 100 × 100 × 100 mm, which were cured for 7 days at 50 °C and hardened for another 7 and 28 days at ambient temperature and dry conditions, were used in these experiments.

2.3. Tests and analyses

The compressive strength of geopolymers was determined using a 2000 kN electro-hydraulic mechanical testing machine. The apparent density of geopolymer samples was determined as the mass of materials per unit volume (Eq. (1)). The mass of geopolymer specimens was also used to calculate the weight loss of geopolymers, after exposure to high temperatures. Three specimens were tested after curing and heating at high temperatures and the average values of the relevant measurements performed for each property are reported in the following tables and figures.

$$\rho = m/V \tag{1}$$

where m(g) and V (cm^3) are the dry mass and apparent volume, respectively, of the geopolymer sample.

The FTIR analysis was performed, using a Fourier Transform IR spectrometer (PerkinElmer 2000 analyzer). The infrared spectra recorded in the wave number range from 650 to 4000 cm^{-1} were collected in the atmosphere, using the Attenuated Total Reflection (ATR) technique with a Zn/Se crystal.

3. Results and discussion

3.1. Syntheses of geopolymers

The geopolymers developed in this study are intended to be used for the passive fire protection of buildings and therefore, their structural stability and mechanical performance at high temperatures are considered particularly significant. Except for the chemical and mineralogical composition of the geopolymer precursor, both these properties are strongly related to important synthesis parameters of geopolymers and specifically, the ratio of solids to liquids (S/L) and the contents of alkali, silicon and aluminum [1,2,21,34]. The S/L ratio controls the rheological properties of the formed geopolymeric paste, such as viscosity and setting time, both of which affect the polymerization and polycondensation processes taking place in geopolymer systems and consequently, the

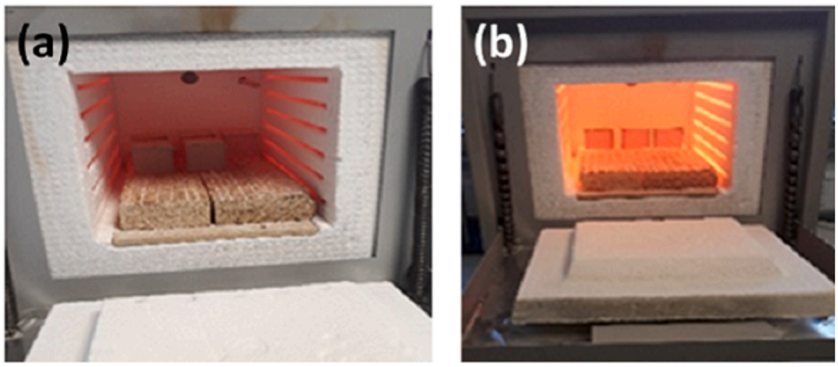

Fig. 5. The used laboratory electric furnace in operation, at (a) 800 °C and (b) 1050 °C.

mechanical properties of the final products. Geopolymeric pastes are considered non-Newtonian fluids with shear thinning behavior (decreasing apparent viscosity with shear rate), reaching very low viscosities at high shear rates [39]. In general, the viscosity of geopolymeric pastes increases and setting time decreases, with the increase of S/L ratio. High S/L ratios under constant conditions result in geopolymeric pastes with high viscosities and short setting times that accelerate the polycondensation process, favoring thus the solidification (hardening) of the formed materials. An increase of S/L ratio increases also the concentrations of Si and Al in the activating solution, enhancing thus the formation of the polymeric binder [3,33,34]. Therefore, the mass of the geopolymeric binder per unit volume of the produced material increases as well, improving the compressive strength of the formed materials. However, the continuous increase of S/L ratio may cause insufficient wetting of the geopolymeric precursor's particles, limiting thus the workability of the formed paste [34].

In general, any geopolymeric system has an optimum range of S/L ratios, which depends on the physicochemical characteristics of the geopolymer precursor and the alkali-activating solution and is defined experimentally, considering the rheological properties and the handling of the resulted geopolymeric paste, as well as the properties of the final materials. In Table 2, the mixing proportions used for the synthesis of the geopolymers investigated in this paper are summarized. The S/L ratios selected for the BFR and CTFR geopolymers were equal to 2.5 g/mL and 3.4 g/mL, respectively, while the volume ratios of $Na_2SiO_3xH_2O$ to KOH solutions in the alkaline activator were kept constant at 1.6 to 1.0 in the mix proportions of both geopolymers (Table 2). During extensive preliminary studies conducted in the laboratory, the above-mentioned ratios have been proven suitable for obtaining geopolymeric pastes with proper rheological properties and final materials with important compressive strength.

3.2. *Effect of CDW type on the compressive strength and physical properties*

Fig. 6 illustrates the compressive strengths of the BFR and CTFR materials, after curing at 50 °C for 7 days and hardening at ambient conditions for 7 and 28 days.

As shown in Fig. 6, both the BFR and CTFR materials developed significant compressive strengths, which proves that geopolymerization has occurred. Moreover, the compressive strength of CTFR was higher than that of BFR, regardless of the hardening time (Fig. 6). The development of compressive strength in geopolymers is strongly related to the extent of the geopolymer binder formation, as well as to the hardness of the geopolymer precursor. In particular, a compromise of these two factors is required for the resulting material to develop high compressive strength. In the current study, both the investigated waste materials contained mineralogical phases that could be dissolved in highly alkaline aqueous solutions. More precisely, the waste ceramic tiles (WCT) comprised an amorphous aluminosilicate phase, albite and mullite (Fig. 4), while the waste bricks (WB) contained alkali feldspars and mullite (Fig. 3), all of which dissolved in the strong alkaline solution used as an activator in this study. The dissolution of aluminosilicate phases in the alkali activator significantly increases Si and Al concentrations, which in turn promotes the formation of Si and/or Si–Al oligomers and their subsequent polycondensation towards the development of an aluminosilicate polymeric network. In a geopolymeric system, this network acts as a binder for the undissolved particles of the geopolymer precursor, which are bound to it during its growth and the entire system hardened to a durable structure, in the following phase of curing. Since the dissolution of the amorphous Al–Si phases in alkaline solutions is faster and equilibrates almost immediately, in comparison to that of the alkali feldspars in

Table 2
Mix designs of the developed geopolymers.

Code name	Precursor (g)		Alkaline Activator					S/L (g/mL)
			Solutions (mL)		Volume Ratios	Molar Ratios		
	WB	WT	KOH	Na_2SiO_3	Na_2SiO_3/KOH	H_2O/K_2O	SiO_2/K_2O	
BFR	2720	–	418	670	1.6 : 1.0	20.5 : 1	2.4 : 1.0	2.5
CTFR	–	2500	283	452	1.6 : 1.0	10.7 : 1	1.2 : 1.0	3.4

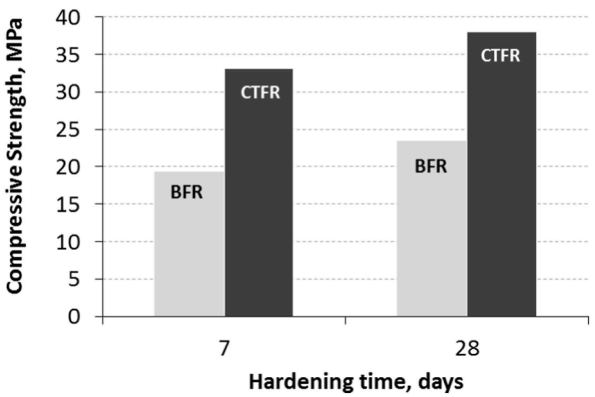

Fig. 6. Compressive strengths of the BFR and CTFR, after curing at 50 °C for 7 days and hardening for 7 and 28 days at ambient conditions.

the same solutions [40–42], the formation of the geopolymer binder in CTFR occurs at a faster rate and to a greater extent from the early stages of the process than in BFR, enhancing thus the development of higher mechanical strength. In addition, the raw sample WCT consisted almost entirely of quartz (Fig. 4) that has a Mohs scale hardness ranging between 7.0 and 7.5, while the WB raw sample contains a significant amount of feldspars, except for quartz (Fig. 3), which decreases the hardness of its particles since the hardness of feldspars ranges between 6 and 6.5 on the Mohs scale. Therefore, the mineralogy of the geopolymer precursors used in this study favors again the development of higher compressive strength in the CTFR geopolymer. According to Fig. 6, increasing the hardening time of both geopolymers by three weeks resulted only to a small improvement in the compressive strength, which was increased by about 1.5 MPa per week for both materials, confirming the unique property of geopolymers to develop remarkable compressive strength from their early stages [1].

The above theoretical approach that correlates the compressive strength of geopolymers with the transformations occurred in their matrix is strengthened by the FTIR analysis of the brick and ceramic tile wastes used in this study and the developed geopolymers, as well. The FTIR spectra of the raw samples of WB and WCT and the corresponding geopolymers BFR and CTFR, after curing at 50 °C for 7 days, are compared in Fig. 7.

The most important bands observed in these FTIR spectra are located at wavenumbers lower than 1250 cm^{-1} (Fig. 7). It concerns the absorption bands assigned to the stretching vibrations of the Si–O–Si and Al–O–Si bonds and can be asymmetric (970–1090 cm^{-1}) and symmetric (650–890 cm^{-1}). Among these bands, the one attributed to the asymmetric stretching vibrations T-O-Si (T = Si or Al) comprises the fingerprint of geopolymerization [34,43–47]. As seen in Fig. 7, this band appeared at around 1010 cm^{-1} and 1020 cm^{-1} in the spectra of the raw samples WB (Fig. 7a) and WCT (Fig. 7c), respectively, while it was shifted to lower wavenumbers in the spectra of the corresponding geopolymers, BFR (Fig. 7b) and CTFR (Fig. 7d), and more precisely, at 978 cm^{-1} and 995 cm^{-1}, respectively. The shifting of this absorption band to lower or higher wavenumbers is a very significant characteristic in geopolymers and consistent with the reorganization of the TO_4 tetrahedra occurring due to the dissolution of aluminosilicate phases and their polymerization in the newly-formed geopolymeric gel-type matrix. Specifically, the shift to lower wavenumbers indicates an increased substitution of Si by tetrahedral Al in the gel matrix [46], improving the mechanical properties of geopolymers. As is seen in Fig. 7d, the peak of this absorption band in the spectrum of CTFR (995 cm^{-1}) was more intensive and sharper than the respective peak in the spectrum of BFR (Fig. 7b) that appeared at 978 cm^{-1}. This observation reveals that the amorphous geopolymeric gel phase formed in the CTFR material was more extended and composed of highly polymerized silica (trimers, rings, planes, etc.) that contained species with bridge Si–O bonds than the terminal, as well as chains of almost similar sizes. On the opposite, the gel phase formed in the BFR material had a limited extent and consisted of polymeric species with a notable variation in chains size [9,47]. Similarly, the absorption band at 877 cm^{-1} in the spectra of the raw samples WB (Fig. 7a) and WCT (Fig. 7c), which is attributed to the symmetric stretching vibrations of Al–O, was shifted to a lower wavenumber (850 cm^{-1}) in the spectra of the geopolymers BFR (Fig. 7b) and CTFR (Fig. 7d). This alteration constitutes an important sign of geopolymerization that is associated with the dissolution of Al-phases through alkali activation and their rearrangement in the formed geopolymer matrix [44,45]. Finally, the disappearance in the spectra of geopolymers of the weak band located at 1160 cm^{-1} in the spectra of raw samples WB and WCT, which is attributed to the vibrational modes of SiO_4 in mullite [2], indicated again the dissolution of aluminosilicate phases from the raw materials in the alkali-activator and their reconstruction in the geopolymer matrix. The same indication also applies to the weak double bands that appeared at 773 cm^{-1} and 796 cm^{-1} in the spectra of both the raw samples WCT and WB and decreased or disappeared in the spectra of the geopolymers CTFR and BFR, respectively. All the above referred transformations are consistent with the formation of a new aluminosilicate phase in geopolymers, which is identical to the alkali-aluminosilicate polymeric network developed in them and constitutes the backbone of their structure. The highly polymerized Al–Si gel and its well-ordered structure (with the predominance of bridge Si–O over terminal Si–O bonds) in CTFR, in comparison to that of the BFR, justifies the development of higher compressive strength in the former material.

The higher compressive strength developed in WCT-based geopolymers is also related to the alterations noted in the absorption band located in-between the wavenumbers 1550 and 1350 cm^{-1} in the FTIR spectra presented in Fig. 7. As shown in Fig. 7, the peaks

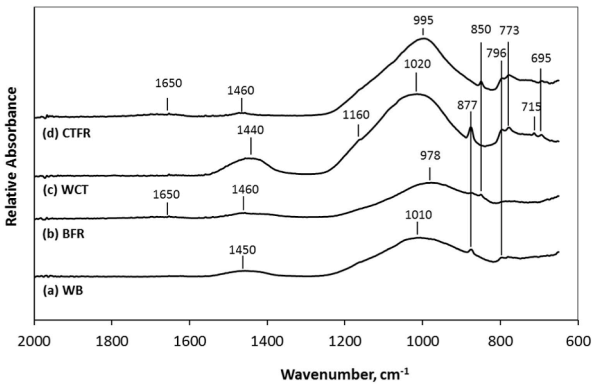

Fig. 7. FTIR spectra of the (a) waste bricks sample (WB), (b) waste brick-based geopolymer (BFR), (c) waste ceramic tiles sample (WCT) and (d) waste ceramic tile-based geopolymer (CTFR) (curing at 50 °C for 7 days and hardening at ambient conditions for 7 days).

appeared in the spectra of the raw samples WB (Fig. 7a) and WCT (Fig. 7c) at 1450 cm^{-1} and 1440 cm^{-1}, respectively, were slightly shifted to circa 1460 cm^{-1}, in the spectra of geopolymers BFR (Fig. 7b) and CTFR (Fig. 7d). Usually, the absorption band appeared at around 1400 cm^{-1} is a characteristic of the C–O–C bonds vibrations, indicating the presence of carbonates in the raw materials and/or the carbonization of the resulted geopolymers [34,44,45,47]. However, this absorption band could also be attributed to the vibrational modes of the Si–O and Al–O bonds [44–46]. As shown in Fig. 7, the relevant peaks are more intense in the raw samples WCT and WB than in the corresponding geopolymers; however, according to their XRD analysis presented in Figs. 3 and 4, respectively, no carbonate mineralogical phases were detected in them. Besides, significant reductions of these peaks were observed in the spectra of the geopolymers BFR (Fig. 7b) and CTFR (Fig. 7d), along with their displacements to higher wavenumber (1460 cm^{-1}). Consequently, the absorption peaks appeared at 1450 and 1440 cm^{-1} in the spectra of WB and WCT, respectively, and are attributed to Si–O and Al–O bonds vibrations and their shifting to 1460 cm^{-1} in the spectra of the corresponding geopolymers is mainly assigned to the dissolution of the aluminosilicate phases existing in WB and WCT and their polymerization in the formed materials [44,47]. As shown in Fig. 7, the reduction of the corresponding peak was greater in the CTFR geopolymer than in the BFR one, thus revealing a larger extent of the newly formed gel-type geopolymeric matrix in the former material and therefore, justifying the development of higher compressive strength. An additional indication for the formation of the geopolymeric binder to a greater extent in CTFR than in BFR, is the peak located at around 1650 cm^{-1} in the spectra of these geopolymers (Fig. 7), which is more intense in the spectrum of CTFR (Fig. 7d) than the one of BFR (Fig. 7b). This peak is attributed to the H–O–H bending vibration mode of the water molecules that are bound on the surface or entrapped in the cavities of the geopolymer network, confirming the formation of the characteristic alkali-aluminosilicate hydrate phase [34,44,45].

In Table 3, the apparent density and mass loss of both geopolymers BFR and CTFR are given, after their curing at 50 °C for 7 days and then, hardening at ambient temperature for 7 and 28 days.

According to Table 3, the mass loss of the WB-based geopolymer (BFR) after hardening for 7 and 28 days was 2.05% and 2.88%, respectively, while the corresponding mass loss percentages of the WCT-based geopolymer (CTFR) were more than double at the same hardening periods. This observation is in agreement with the analysis made above for the extent of gel formation in the developed geopolymers. As revealed by FTIR analysis, the formation of Al–Si hydrate phases in CTFR was much higher than that in the BFR (Fig. 7); the dehydration of these phases was favored with the increase of curing time, leading to higher mass losses for the CTFR material. Consequently, after a hardening period of 28 days, the decrease of the CTFR density was much higher than that of the BFR density (Table 3).

3.3. Effect of high temperatures on the compressive strength and physical properties

Since the CDW-based geopolymers developed in this study aim to be used as fireproofing materials for the passive fire protection of buildings, their mechanical strength and structural stability at high temperatures are considered particularly important. Figs. 8 and 9 present the residual compressive strengths of the geopolymers BFR and CTFR, respectively, after their exposure to the studied high temperatures. Both materials were cured at 50 °C for 7 days and hardened at ambient temperature for 7 and 28 days, before being ex-

Table 3
Physical properties of the prepared geopolymers.

Geopolymer code name	Density (kg/m^3)		Mass loss (%)	
	Hardening time			
	7 days	28 days	7 days	28 days
BFR	1554	1526	2.05	2.88
CTFR	1743	1621	4.36	7.01

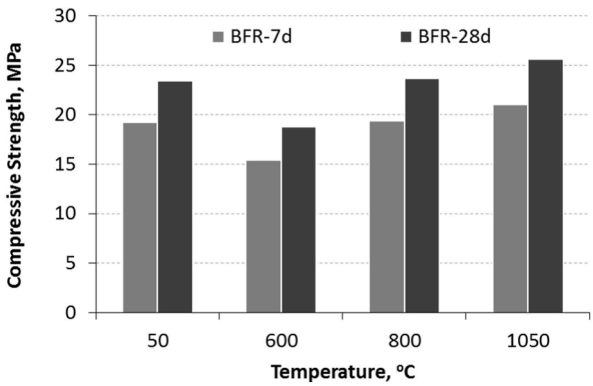

Fig. 8. Residual compressive strengths of the BFR geopolymer after exposure to high temperatures for 2 h (curing at 50 °C for 7 d; hardening at ambient temperature for 7 and 28 days).

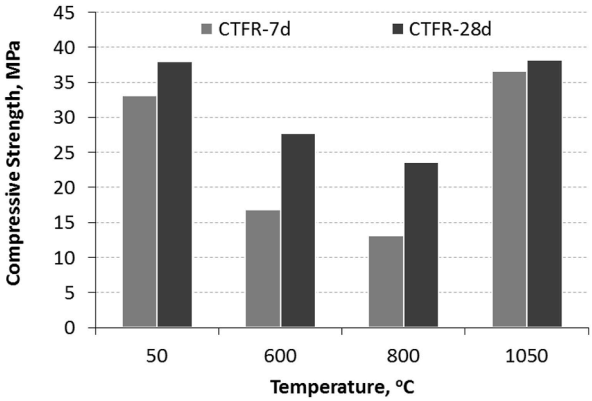

Fig. 9. Residual compressive strengths of the CTFR geopolymer after exposure to high temperatures for 2 h (curing at 50 °C for 7 d; hardening at ambient temperature for 7 and 28 days).

posed at the studied high temperatures. Figs. 8 and 9 include also the compressive strengths of BFR and CTFR, respectively, after their curing and hardening, in order to serve as the reference value.

According to Fig. 8, after the exposure of BFR at 600 °C, the residual compressive strength was approximately 75% of its strength after curing. When the same material was exposed at 800 °C, its compressive strength was quite similar to that before the heating treatment (Fig. 8), while it was slightly increased after the material's exposure to the highest tested temperature of 1050 °C. As shown in Fig. 8, the increase of the hardening period also increased the residual compressive strength of BFR upon firing at the different temperatures, by a similar percentage (~22%).

Regarding CTFR geopolymer, its residual compressive strength at 600 °C was about 50% of that of the unheated material, as shown in Fig. 9. The residual strength further decreased, after the specimens' exposure at 800 °C, retaining about 40% of the strength value it had before any thermal treatment (Fig. 9). Further increase of the exposure temperature to 1050 °C involved a sharp increase in the residual compressive strength of CTFR, in comparison to the one measured after exposure at 800 °C and also a very small improvement, in comparison to the strength of the unheated material (increased by about 10%) (Fig. 9). As the hardening time of the unheated specimens was increased from 7 to 28 days, the residual compressive strength of CTFR increased by about 10 MPa, after firing at 600–800 °C. At the highest investigated temperature of 1050 °C, the residual compressive strength remained almost unchanged, regardless the hardening time (Fig. 9).

The changes in the compressive strength of BFR and CTFR geopolymers observed after their exposure at the studied elevated temperatures are related to structural rearrangements that took place in their matrices, due to water evaporation, dehydroxylation and phase transformations [48–50]. The decrease in the compressive strength observed after the thermal treatment of BFR (Fig. 8) and CTFR (Fig. 9) at 600 °C can be attributed to the vapour pressure effect taking place in the geopolymeric matrix, due to the dehydration and dehydroxylation of the alkali-silicate-aluminate hydrate phases conducted at this temperature. During the heating of geopolymers at around 300 °C, the physically and chemically bonded water in the geopolymeric matrix evaporated gradually [49], while at temperatures above 300 °C and up to about 600 °C, dehydroxylation of the silanol (>Si–OH) and aluminol (>Al–OH) groups also occurred [48]. The removal of water molecules and hydroxyl ions from the geopolymeric matrix disarranged the polymeric network, while the formed vapour, in combination with the heat transferring, involved the gradual growth in pore pressure inside the geopolymeric gel-type phase. When this pressure exceeded a maximum limit for the capillary of the geopolymeric gel phase and given the low permeability and the micro-to nano-porosity of geopolymers [1,6], an intensive micro-cracking occurred inside the materials, leading to a significant reduction in their mechanical strength. Except for the aforementioned vapour effect, the softening of the alkali-aluminosilicate gel phase that starts at around 500–550 °C [49], as well as the alpha-beta transition of quartz taking place at 573 °C [26], also contributed to the decrease in compressive strength of both the geopolymers. Indeed, the larger extent of geopolymerization that took place in CTFR, rather than in BFR, as was argued above, and the predominance of quartz in the raw sample of WCT (Fig. 4) could reasonably expalin and justify the sharper decrease in the compressive strength of WCT noted at 600 °C.

The important changes in pore structure occurred at higher temperatures due to sintering of the geopolymeric matrix have also affected the mechanical strength of both the studied geopolymers. Between temperatures of 550 and 900 °C, the alkali-aluminosilicate gel-type phase of geopolymers forms a viscous binder that sinters the solid particles of the geopolymeric precursor through diffusion in the contact zone of their boundaries [26]. Sintering reduces the porosity of materials and promotes the increasing in their mechanical strength [29,30,48,49], as it results in the densification of the geopolymeric matrix into a glass- or ceramic-like structure [50]. The viscous geopolymeric gel phase that is formed fills the existing pores in the geopolymeric matrix, while at high temperatures leads also to crack healing [26,50]. As shown in Fig. 8, BFR geopolymer regained its initial compressive strength after exposure at 800 °C, due to the sintering occurred in its matrix. The compressive strength of BFR remained almost constant after its exposure at 1050 °C, as well (Fig. 8), which indicates the completion of the sintering process and the solidification of the material. On the opposite, the sintering appeared to be incomplete at 800 °C in the case of CTFR (Fig. 9), which comprises an additional indication of the greater degree of polymerization that occurred in this material. The high amount of the formed geoplymeric binder in CTFR decelerated the interparticle binding process and thus, increased the temperature of the viscous sintering completion, as seen in Fig. 9. The sharp increase of the CTFR compressive strength noted after its exposure at 1050 °C (Fig. 9) confirms this consideration. In general, after the comple-

tion of sintering, geopolymers remain stable up to 1200–1400 °C, depending on the melting point of the crystalline phases such as nepheline, kalsilite, mullite or leucite that are formed in their matrices at temperatures above 800 °C [26,29,30,37].

The above-mentioned microstructural changes that took place in geopolymers after their firing at the studied high temperatures, and therefore affecting their mechanical strength, were also confirmed through the FTIR analysis. The relevant FTIR spectra of BFR and CTFR geopolymers are presented in Figs. 10 and 11, respectively. As shown in Figs. 10 and 11, the absorption band that appeared at 1650 cm^{-1} in the spectra of the unheated geopolymers BFR and CTFR, respectively and was attributed to the vibration of the H–O–H bonds in the water molecules, has been eliminated in the spectra of the corresponding geopolymers, after their heating at 600 °C (Figs. 10b and 11b, respectively). Accordingly, the peaks related to the hydroxyl-ion bonds vibrations that appeared at the wavenumbers 1460 cm^{-1} (Si–O and Al–O bonds vibration) and 850 cm^{-1} (Al–O bond vibration) in the spectra of BFR and CTFR geopolymers shown in Figs. 10a and Fig. 11a, respectively, disappeared in the spectra corresponding to BFR and CTFR after their exposure to 600 °C (Figs. 10b and 11b, respectively).

The structural rearrangements that occurred due to the sintering and densification of the geopolymeric gel phase and have taken place during the exposure of both geopolymers at 800 °C, were also revealed through FTIR analysis. As seen in Fig. 10, the absorption band of T-O-Si stretching vibration that was located at 978 cm^{-1} in the spectrum of BFR (Fig. 10a) moved to lower wavenumber (939 cm^{-1}), after the exposure of BFR at 600 °C (Fig. 10b), indicating enhanced polymerization. The same absorption band moved again to a higher wavenumber (966 cm^{-1}), after the exposure of BFR at 800 °C (Fig. 10c), denoting recrystallization of the geopolymeric gel phase [26,32]. The above structural changes are consistent with the initial decrease and the subsequent increase of the compressive strength of BFR, after its exposure at 600 and 800 °C, respectively (Fig. 8). The broad band found at the wavenumbers 1200–800 cm^{-1} in BFR spectrum after heating of the material at 1050 °C (Fig. 10d) implied lower polymerized silica, which justifies the very small improvement in the compressive strength of the relevant material (Fig. 8).

Similarly, in the spectra of CTFR geopolymer, the absorption band of T-O-Si stretching vibrations that was located at 995 cm^{-1}, before and after heating the material at 600 °C (Fig. 10a and b, respectively), shifted slightly to higher wavenumbers after the exposure of CTFR at 800 and 1050 °C (Fig. 10c and d, respectively). This shifting indicated the sintering of the aluminosilicate gel phase and the crystallization of new phases [43,44], which improved in turn the compressive strength of CTFR at 1050 °C (Fig. 9).

The dehydration and dehydroxylation of the alkali-silicate-aluminate hydrate phases occurring at temperatures up to 600 °C imply a significant reduction in the materials' mass and consequently, in their density. Taking into account the properties of the unheated geopolymers (Table 3), the BFR geopolymers that were hardened for 7 and 28 days presented a mass loss of about 6% and 8%,

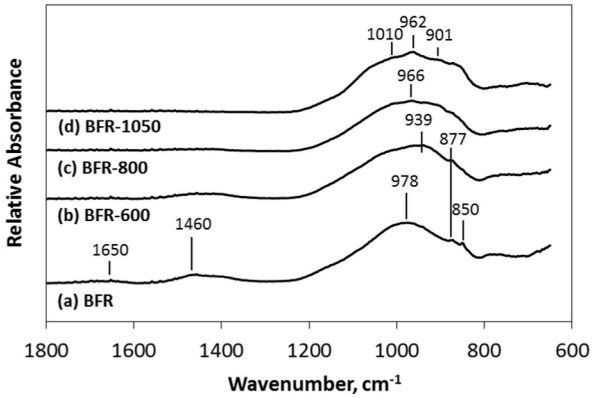

Fig. 10. FTIR spectra of the BFR geopolymer after (a) curing at 50 °C for 7 d and exposure for 2 h to (b) 600 °C, (c) 800 °C and (d) 1050 °C.

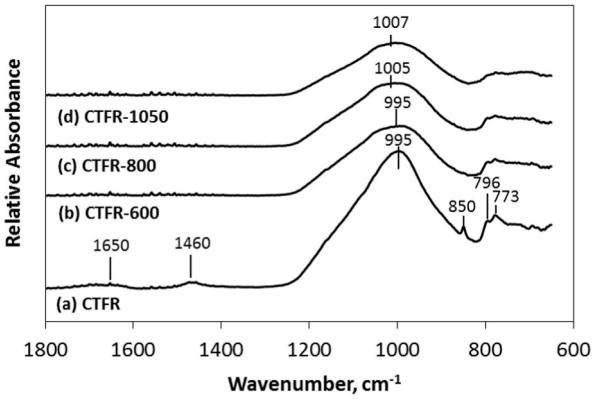

Fig. 11. FTIR spectra of the CTFR geopolymer after (a) curing at 50 °C for 7 d and exposure for 2 h to (b) 600 °C, (c) 800 °C and (d) 1050 °C.

Table 4
Properties of the BFR and CTFR geopolymers after exposed at high temperatures.

Geopolymer code name	Temperature (°C)	Density (kg/m³)		Mass loss (% wt)	
		Hardening time			
		7 days	28 days	7 days	28 days
BFR	50	1554	1526	2.05	2.88
	600	1475	1476	6.21	7.81
	800	1430	1431	7.53	9.46
	1050	1434	1437	7.97	10.02
CTFR	50	1743	1621	4.36	7.01
	600	1583	1579	9.55	13.02
	800	1569	1578	9.60	13.19
	1050	1578	1566	9.91	13.55

respectively, after their exposure at 600 °C (Table 4), while the corresponding mass loss in the case of the CTFR geopolymers, was between 10% and 13%, as seen in Table 4. At this temperature, the apparent density of the unheated BFR (Table 3) was slightly reduced by almost 50–80 kg/m³ (Table 4), while in the case of the CTFR geopolymer, the reduction of density was about 160 kg/m³, which is almost twice larger than that of the BFR geopolymer (Table 4). Despite the significant microstructural changes that occurred in geopolymers in the temperature range of 200–600 °C, only a few small cracks were observed on the specimens' surfaces of both the BFR and CTFR geopolymers, after their exposure at 600 °C (Fig. 12). These cracks were more visible on the surface of BFR specimens.

The thermal exposure of geopolymers at 800 °C resulted in a small decrease in their density and an increase in their mass loss (Table 4), which both are related to the sintering and densification of the geopolymeric matrices. The weak increase in the density of both geopolymers noted after their exposure at 1050 °C, even though both of the materials presented a small mass loss (Table 4), is attributed to the formation of new crystalline phases [26,27].

Only a few intensive cracks, without any other sign of spalling or deformation, were visible on the specimens' surface of both geopolymers, after their firing at 800 ° C (Fig. 12). It is important to note that these cracks disappeared from both geopolymers after their exposure at 1050 °C, due to self-healing by the sintering of the viscous geopolymeric gel phase that took place at this temperature [32].

4. Conclusions

From the present research study, the following conclusions are summarized.

- The geopolymers based entirely on waste cricks and waste ceramic tiles were proved stable after their exposure to elevated temperatures up to 1050 °C. Only a few surface cracks were visible, after the exposure of the geopolymers at 600 °C. The observed cracks became more intensive after exposure at 800 °C and disappeared from both of the geopolymers after their exposure at 1050 °C, due to self-healing phenomena that are related to the sintering of the geopolymeric gel phase.
- The significant decreases in the materials' compressive strength and density observed after their exposure at 600 °C were attributed to the structural changes that took place in the geopolymeric matrices, due to dehydration and dehydroxylation processes. The higher degree of geopolymerization in the waste ceramic tile-based material resulted in more intense decreases in the compressive strength and density, than the corresponding values in the waste brick-based one.
- The sintering process that took place in the geopolymeric matrix above 600 °C increased the compressive strength of the waste brick-based geopolymer, after its exposure at 800 °C. This strength improvement was decelerated in the case of waste ceramic tile-based material, due to the higher degree of geopolymerization. At 1050 °C, the compressive strengths of both materials were further improved and reached almost the reference values of the unheated specimens.
- The investigated geopolymers have the potential to be effectively used for the passive fire protection of buildings. Their good thermal and mechanical performance at high temperatures, in combination with the utilization of waste materials for their production, the remarkably low processing temperature and carbon footprint, make them very attractive as fire-resistant materials. In this direction, it is necessary to define their exact applications and the relevant specifications, while further investigation for their up-scaling is required.

CRediT author statement

Ioanna Giannopoulou: Conceptualization, Methodology, Data curation, Investigation, Writing - original.
Ponsian M. Robert: Experimental investigation, Data curation.
Konstantinos-Miltiadis Sakkas: Investigation, Methodology.
Michael F. Petrou: Investigation, Reviewing.
Demetris Nicolaides: Supervision, Conceptualization, Reviewing, Project Administration.

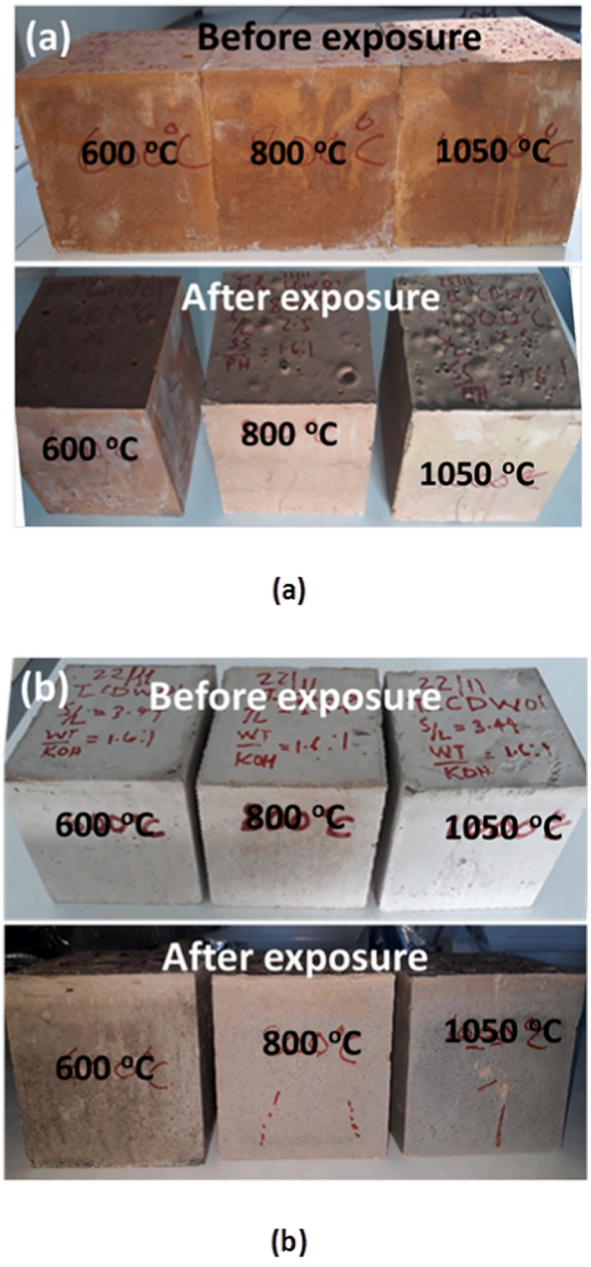

Fig. 12. The (a) BFR and (b) CTFR geopolymers before and after exposure to elevated temperatures.

Declaration of competing interest

The authors declare that they have no known competing financial interests or personal relationships that could have appeared to influence the work reported in this paper.

Data availability

Data will be made available on request.

Acknowledgements

This investigation is performed under the research project entitled "Development of an Innovative Insulation Fire Resistant Façade from the Construction and Demolition Wastes - DEFEAT" (INTEGRATED/0918/0052), which has been co-funded by the European Regional Development Fund (ERDF) and the Cyprus Government, through the RESTART 2016–2020 framework program of the Cyprus Research & Innovation Foundation.

References

[1] J. Davidivits, Geopolymers, J. Therm. Anal. 37 (8) (1991) 1633–1656, https://doi.org/10.1007/BF01912193.
[2] [24]: D. Khale, R. Chaudhary, Mechanism of geopolymerization and factors influencing its development: a review, J. Mater. Sci. 42 (2007) 729–746, https://doi.org/10.1007/s10853-006-0401-4.
[3] M. Zhang, T. El-Korchi, G. Zhang, J. Liang, M. Tao, Synthesis factors affecting mechanical properties, microstructure, and chemical composition of red mud-fly ash based geopolymers, Fuel 134 (2014) 315–325, https://doi.org/10.1016/j.fuel.2014.05.058.
[4] W. Hajjaji, S. Andrejkovičová, C. Zanelli, M. Alshaaer, M. Dondi, J.A. Labrincha, F. Rocha, Composition and technological properties of geopolymers based on metakaolin and red mud, Mater. Des. 52 (2013) 648–654, https://doi.org/10.1016/j.matdes.2013.05.058.
[5] Y. Wu, B. Lu, Z. Yi, F. Du, Y. Zhang, The properties and latest application of geopolymers, IOP Conf. Ser. Mater. Sci. Eng. 472 (2019) 012029, https://doi.org/10.1088/1757-899X/472/1/012029.
[6] P. Duxson, A. Fernandez-Jimenez, J.L. Provis, G.C. Lukey, A. Palomo, J.S.J. van Deventer, Geopolymer technology: the current state of the art, J. Mater. Sci. 42 (2007) 2917–2933.
[7] M. Alhawat, A. Ashour, G. Yildirim, A. Aldemir, M. Sahmaran, Properties of geopolymers sourced from construction and demolition waste: a review, J. Build. Eng. 50 (2022) 104104, https://doi.org/10.1016/j.jobe.2022.104104.
[8] H.Y. Zhang, V. Kodur, S.L. Qi, L. Cao, B. Wua, Development of metakaolin–fly ash based geopolymers for fire resistance applications, Construct. Build. Mater. 55 (2014) 38–45.
[9] I. Giannopoulou D. Panias Maragkos, Synthesis of ferronickel slag-based geopolymers, Miner. Eng. 22 (2009) 196–203, https://doi.org/10.1016/j.mineng.2008.07.003.
[10] Y. Pontikes, L. Machiels, S. Onisei, L. Pandelaers, D. Geysen, P.T. Jones, B. Blanpain, Slags with a high Al and Fe content as precursors for inorganic polymers, Appl. Clay Sci. 73 (2013) 93–102, https://doi.org/10.1016/j.clay.2012.09.020.
[11] T. Bakharev, Thermal behaviour of geopolymers prepared using class F fly ash and elevated temperature curing, Cement Concr. Res. 36 (6) (2006) 1134–1147, https://doi.org/10.1016/j.cemconres.2004.06.031.
[12] T.W. Cheng, J.P. Chiu, Fire-resistant geopolymer produced by granulated blast furnace slag, Miner. Eng. 16 (2003) 205–210, https://doi.org/10.1016/S0892-6875(03)00008-6.
[13] J. Davidovits, Fire proof geopolymeric cements, in: Proceedings of Second International Conference Geopolymere, 1999, pp. 165–169.
[14] K. Komnitsas, D. Zaharaki, G. Bartzas, Effect of sulphate and nitrate anions on heavy metal immobilisation in ferronickel slag geopolymers, Appl. Clay Sci. 73 (2013) 103–109, https://doi.org/10.1016/j.clay.2012.09.018.
[15] J.Z. Xu, Y.L. Zhou, Q. Chang, H.Q. Qu, Study on the factors of affecting the immobilization of heavy metals in fly ash-based geopolymers, Mater. Lett. 60 (6) (2006) 820–822, https://doi.org/10.1016/j.matlet.2005.10.019.
[16] Z. Yunsheng, S. Wei, C. Qianli, C. Lin, Synthesis and heavy metal immobilization behaviors of slag based geopolymers, J. Hazard Mater. 143 (1–2) (2007) 206–213.
[17] H. Xu, J.S.J. van Deventer, The geopolymerization of alumino-silicate minerals, Int. J. Miner. Process. 59 (2000) 247–266, https://doi.org/10.1016/S0301-7516(99)00074-5.
[18] P.V. Krivenko, G.Yu Kovalchuk, Directed synthesis of alkaline aluminosilicate minerals in a geocement matrix, J. Mater. Sci. 42 (2007) 2944–2952.
[19] S. Luhar, T.-W. Cheng, D. Nicolaides, I. Luhar, D. Panias, K. Sakkas, Valorisation of glass waste for development of Geopolymer composites – mechanical properties and rheological characteristics: a review, Construct. Build. Mater. 220 (2019) 547–564, https://doi.org/10.1016/j.conbuildmat.2019.06.041.
[20] Ch Baia, H. Lic, E. Bernardo, P. Colombo, Waste-to-resource preparation of glass-containing foams from geopolymers, Ceram. Int. 45 (2019) 7196–7202, https://doi.org/10.1016/j.ceramint.2018.12.227.
[21] K. Komnitsas, D. Zaharaki, A. Vlachou, G. Bartzas, M. Galetakis, Effect of synthesis parameters on the quality of construction and demolition wastes (CDW) geopolymers, Adv. Powder Technol. 26 (2015) 368–376, https://doi.org/10.1016/j.apt.2014.11.012.
[22] A. Allahverdi, E.N. Kani, Construction wastes as raw materials for geopolymer binders, Int. J. Civ. Eng. 7 (3) (2009) 154–160.
[23] D. Kioupis, A. Skaropoulou, S. Tsivilis, G. Kakali, Valorization of brick and glass CDWs for the development of geopolymers containing more than 80% of wastes, Minerals (2020), https://doi.org/10.3390/min10080672.
[24] A.R.G. Azevedo, C.M.F. Vieira, W.M. Ferreira, K.C.P. Faria, L.G. Pedroti, B.C. Mendes, Potential use of ceramic waste as precursor in the geopolymerization reaction for the production of ceramic roof tiles, J. Build. Eng. 29 (2020) 101156, https://doi.org/10.1016/j.jobe.2019.101156.
[25] European Commission, Development and Implementation of Initiatives Fostering Investment and Innovation in Construction and Demolition Waste Recycling Infrastructure, Publications Office of the European Union, 2018, https://doi.org/10.2873/11837.
[26] M. Lahoti, K.H. Tan, E.-H. Yang, A critical review of geopolymer properties for structural fire-resistance applications, Construct. Build. Mater. 221 (2019) 514–526, https://doi.org/10.1016/j.conbuildmat.2019.06.076.
[27] P. Duxson, G.C. Lukey, J.S.J. van Deventer, The thermal evolution of metakaolin geopolymers: Part 2 – phase stability and structural development, J. Non-Cryst. Solids 353 (22) (2007) 2186–2200, https://doi.org/10.1016/j.jnoncrysol.2007.02.050.
[28] G.Y. Kovalchuk, P.V. Krivenko, Producing fire- and heat-resistant geopolymers, in: J.L. Provis, J.S.J. van Deventer (Eds.), Geopolymers Structure, Processing, Properties and Industrial Applications, Woodhead Publishing, 2009, pp. 227–266.
[29] V.F.F. Barbosa, K.J.D. MacKenzie, Synthesis and thermal behaviour of potassium sialate geopolymers, Mater. Lett. 57 (9) (2003) 1477–1482, https://doi.org/10.1016/S0167-577X(02)01009-1.
[30] V.F.F. Barbosa, K.J.D. MacKenzie, Thermal behaviour of inorganic geopolymers and composites derived from sodium polysialate, Mater. Res. Bull. 38 (2) (2003) 319–331, https://doi.org/10.1016/S0025-5408(02)01022-X.
[31] P. Duxson, G. Lukey, J.J. van Deventer, Physical evolution of Na-geopolymer derived from metakaolin up to 1000 ^{o}C, J. Mater. Sci. 42 (9) (2007) 3044–3054, https://doi.org/10.1007/s10853-006-0535-4.
[32] M. Lahoti, K.K. Wong, K.H. Tan, E.-H. Yang, Effect of alkali cation type on strength endurance of fly ash geopolymers subject to high temperature exposure, Mater. Des. 154 (2018) 8–18, https://doi.org/10.1016/j.matdes.2018.05.023.
[33] Y.M. Liew, H. Kamarudin, A.M.M. Al Bakri, M. Bnhussain, M. Luqman, I.K. Nizar, C.M. Ruzaidi, C.Y. Heah, Optimization of solids-to-liquid and alkali activator ratios of calcined kaolin geopolymeric powder, Construct. Build. Mater. 37 (2012) 440–451, https://doi.org/10.1016/j.conbuildmat.2012.07.075.
[34] D. Panias, I. Giannopoulou, Th Perraki, Effect of synthesis parameters on the mechanical properties of fly ash-based geopolymers, Colloids Surf. A Physicochem. Eng. Asp. 301 (2007) 246–254, https://doi.org/10.1016/j.colsurfa.2006.12.064.
[35] P. Rovnanik, P. Bayer, P. Rovnanikova, Characterization of alkali activated slag paste after exposure to high temperatures, Construct. Build. Mater. 47 (2013) 1479–1487, https://doi.org/10.1016/j.conbuildmat.2013.06.070.
[36] K.-M. Sakkas, P. Nomikos, A. Sofianos, D. Panias, Inorganic polymeric materials for passive fire protection of underground constructions, J. Fire Mater. 37 (2013) 140–150, https://doi.org/10.1002/fam.2119.
[37] K.-M. Sakkas, A. Sofianos, P. Nomikos, D. Panias, Behaviour of fire protection K-geopolymer under successive severe incidents, Materials 8 (9) (2015) 6096–6104, https://doi.org/10.3390/ma8095294.
[38] M. Guerrieri, G.J. Sanjayan, Behaviour of combined fly ash/slag based geopolymers when exposed to high temperatures, Fire Mater. 34 (2010) 163–175, https://doi.org/10.1002/fam.1014.
[39] Y. Rifaai, A. Yahia, A. Mostafa, S. Aggoun, El-H. Kadri, Rheology of fly ash-based geopolymer: effect of NaOH concentration, Construct. Build. Mater. 223 (2019) 583–594, https://doi.org/10.1016/j.conbuildmat.2019.07.028.
[40] K.G. Knauss, T.J. Wolery, Dependence of albite dissolution kinetics on ph and time at 25°c and 70°c, Geochem. Cosmochim. Acta 50 (11) (1986) 2481–2497, https://doi.org/10.1016/0016-7037(86)90031-1.
[41] T. Antonic, A. Cizmek, C. Kosanovic, B. Subotic, Dissolution of amorphous aluminosilicate zeolite precursors in alkaline solutions Part 1.-Kinetics of the dissolution, J. Chem. Soc., Faraday Trans. 89 (1993) 1817–1822 10/1039/FT9938901817.

[42] G. Yuan, Y. Cao, H.-M. Schulz, F. Hao, J. Gluyas, K. Liu, T. Yang, Y. Wang, K. Xi, F. Li, A review of feldspar alteration and its geological significance in sedimentary basins: from shallow aquifers to deep hydrocarbon reservoirs, Earth Sci. Rev. 191 (2019) 114–140, https://doi.org/10.1016/j.earscirev.2019.02.004.
[43] A. Valouma Soultana, G. Bartzas, K. Komnitsas, Properties of inorganic polymers produced from brick waste and metallurgical slag, Minerals 9 (2019) 551, https://doi.org/10.3390/min9090551.
[44] Fernandez-Jimenez, A. Palomo, Mid-infrared spectroscopic studies of alkali activated fly ash structure, Microporous Mesoporous Mater. 86 (2005) 207–214, https://doi.org/10.1016/j.micromeso.2005.05.057.
[45] A. Rees, J.L. Provis, G.C. Lukey, J.S.J. van Deventer, Attenuated total reflectance fourier Transform infrared analysis of fly ash geopolymer gel aging, Langmuir 23 (2007) 8170–8179, https://doi.org/10.1021/la700713g.
[46] M. Criado, A. Fernandez-Jimenez, A. Palomo, Alkali activation of fly ash: effect of the SiO2/Na2O ratio Part I: FTIR study, Microporous Mesoporous Mater. 106 (2007) 180–191, https://doi.org/10.1016/j.micromeso.2007.02.055.
[47] G. Socrates, Infrared and Raman Characteristic Group Frequencies, third ed., John Wiley & Sons Ltd., Chichester, UK, 2001.
[48] R. He, N. Dai, Z. Wang, Thermal and mechanical properties of geopolymers exposed to high temperature: a literature review, Adv. Civ. Eng. (2020) https://doi.org/10.1155/2020/7532703, ID: 7532703.
[49] J.S.J. Van Deventer, J.L. Provis, P. Duxson, G.C. Lukey, Reaction mechanisms in the geopolymeric conversion of inorganic waste to useful products, J. Hazard Mater. 139 (3) (2007) 506–513, https://doi.org/10.1016/j.jhazmat.2006.02.044.
[50] R. Ahmad, W.M.W. Ibrahim, M.M.A.B. Abdullah, P. Pakawanit, P. Vizureanu, A.S. Abdullah, A.V. Sandu, F.H. Ahmad Zaidi, Geopolymer-based nepheline ceramics: effect of sintering profile on morphological characteristics and flexural strength, Crystals 12 (2022) 1313, https://doi.org/10.3390/cryst12091313.